Numerical Investigation of Nanofluid's Heat Transfer Performance in Passive Residual Heat Removing System of AP1000 Nuclear Reactor

MANTASHA PONKTY[1], ANAMIKA PUJA[2], ABDUS SATTAR MOLLAH[1,*]
[1]Department of Nuclear Science and Engineering,
Military Institute of Science and Technology,
Dhaka,
BANGLADESH

[2]Department of Energy and Nuclear Engineering,
Ontario Tech University,
Oshawa,
CANADA

**Corresponding Author*

Abstract: - The Passive Heat Removal system (PHRS) is designed to remove the residual heat from the core in case of a station blackout, failure of emergency core cooling system, or failure of feedwater supply through the Passive Residual Heat Removal Heat Exchanger (PRHR HX). PRHR HX consists of a C-shaped tube bundle as a heat exchanger and the In-Containment Refueling Water Storage Tank (IRWST) as a heat sink. A temperature distribution of this passive heat removal system of an AP1000 Reactor is generated using COMSOL Multiphysics and the heat transfer coefficient is calculated to illustrate the effectiveness of the PHRS. A comparison of the heat transfer coefficient between the IRWST filled with water and nanofluid has been generated using the PRHR HX design. Thermophysical properties of nanofluids have been calculated in the process of calculating the heat transfer coefficient. Numerical results show the difference in temperature reduction of Al_2O_3, TiO_2, and Ag as opposed to water in the IRWST. Time-dependent heat conduction of water and nanofluid results contribute to the effective analysis of passive heat removal systems and provide information for the safe operation of AP1000 reactors. By the end of 2024/2025, two VVER-1200 power stations with a combined capacity of 2400 MW will be operating in Bangladesh. For safety and licensing reasons, heat transfer simulation of VVER-1200 can be performed using COMSOL software.

Key-Words: - Passive Heat, Nanofluid, Heat Transfer, PRHR Hx, AP1000, COMSOL, CFD, IRWST, Mesh.

Received: September 12, 2023. Revised: May 17, 2024. Accepted: June 13, 2024. Published: July 31, 2024.

1 Introduction

Global public anxiety over the safety of nuclear reactor operations has skyrocketed in the wake of the Fukushima Daiichi tragedy in 2011. Due to the loss of power to pump cooling water, the accident's leftover heat from the core cannot be dissipated in time. Therefore, the primary focus in recent years has been on creating novel and sophisticated reactors with passive safety features. Without any further active controls or activities, the passive safety systems can function. The fundamental laws of physics serve as the engine for the continuous operation of passive safety measures. There are numerous designs of large Gen-II/III+ Pressurized Water Reactors on the market. Technologies such as the Korean APR-1400, European EPR, American AP1000, Russian VVER-1200, NHR-200-II in China and others, [1], [2], [3], [4]. Many modern pressurized water reactors (PWRs) have used the passive residual heat removal heat exchanger (PRHR HX) with a C-tube bundle in recent years. The PRHR HX is a crucial piece of equipment in the passive safety system that is housed in the in-containment refilling water storage tank (IRWST) of the AP1000 (a two-loop advanced passive power plant) and CAP1400 (a two-loop advanced passive power plant) in China. For the reactor's safety, the Passive Residual Heat Removal System's (PRHRS) efficient and dependable operation is crucial. The PRHR HX's (passive residual heat removal heat exchanger) heat transfer effect is negatively

impacted by the stratification that can occur in the passive heat sink tank (IRWST) of the PRHRS. The Westinghouse AP1000 was the main focus of the authors' attention in this paper, [2], [3], [4].

AP1000 Pressurized Water Reactors use passive safety systems to enhance plant safety and these systems use only natural forces such as gravity, natural circulation, and compressed gas to provide the driving forces for the systems to adequately cool the reactor core following an accident. As a part of the Passive Safety System (PSS), the Passive Residual Heat Removal System (PRHRS) removes the decay heat from the core by natural circulation. PRHRS is composed of a heat source and heat sink with a piping system between two components allowing water to circulate due to the buoyancy effect, [5], [6], [7]. In-Containment Refueling Water Storage Tank (IRWST) works as a heat sink and the primary coolant water is the heat source in this system releasing heat through the C-shaped tube bundle heat exchanger immersed into the IRWST. A passive residual heat removal heat exchanger is a key equipment in the passive residual heat removal system, which plays an important role in the safety of the reactor in any emergency or accidental scenario.

Authors [8] analyzed the heat transfer and flow calculation of the PRHR Hx of the AP1000 reactor. In this study, RELAP5 is applied to calculate heat distribution, and ANSYS FLUENT codes are used to obtain the CFD calculations. To increase the heat transfer capacity of the system, the implementation of nanofluid in the IRWST has good research potential due to its proven effectiveness in heat-exchanging applications.

To study the heat transfer enhancement, three nanofluids are considered in this research- Ag-water, TiO_2-water, and Al_2O_3-water nanofluids. These nanofluids show better thermal properties compared to their base-fluid water. Authors [9] studied the thermal conductivity enhancement of aqueous solution of silver nanoparticles. Authors [10] experimentally researched thermo-physical properties and heat transfer characteristics of low-volume fraction water-based silver nanofluid. Thermal conductivity and viscosity of TiO2-water nanofluid are measured, [11]. Heat transfer enhancement by applying TiO_2 nanofluid is experimentally proved by researchers, [12]. Authors [13] studied the properties of both water and ethylene glycol-based Al_2O_3 nanofluid depending on the temperature and concentration as well as their effect on free convective heat transfer. Finally, the established and proposed correlations of nanofluid properties and enhancement ratios of thermal characteristics of water-based composite nanofluids discussed in different studies are reviewed by researchers, [14].

With the advancement of science, the production of nanoparticles from various materials has become possible. One of the characteristics of materials in the scale of nano is the large surface-to-volume ratio, which gives them special abilities. Nanofluid is a term proposed by researcher [15] as a new kind of heat transfer fluid that contains small quantities of metallic or non-metallic nanoparticles. These particles were scattered homogeneously and permanently in a continuous phase. Other researchers [16] explored the theoretical approach of nanoparticles and their properties in terms of using them in heat exchangers for enhanced efficiency.

Researcher [17] numerically experimented with the flow and heat transfer of nanofluid for the application of solar collectors. Two types of nanofluids were chosen in the study- CuO and Al_2O_3 in volume fractions of 0.5% and 1%. With COMSOL Multiphysics simulations, it was possible to prove the result to accord with the theory of Nanofluid's enhanced heat transfer behavior.

In recent years, there have been a significant number of studies on Passive Heat Removing Systems. Authors [18] numerically investigated the behavior of the ultimate heat sink whereas other researchers [19], [20] showed heat transfer and fluid flow studies in both numerical and experimental approaches. To improve the heat transform performance, researchers [21] suggested an outstanding idea of change in PRHR Hx tube design and introduced a spiral shape instead of regular C-shape submerged tubes. In our study, nanofluid is applied as the ultimate heat sink, keeping the regular C-shape of the PRHR Hx tubes to compare the performance of the heat-removing system with the regular setup of the water heat sink.

The application of nanofluid in the Passive Heat System of nuclear power plants is a potential research area that can bring out the possibility of elevating heat transfer in a passive approach. Adequate research can help to find out the most suitable nanofluid with optimized concentration which can be used to achieve the goal.

Numerous studies involving nuclear reactors have made use of COMSOL Multiphysics to carry out multiphysics simulations like thermal hydraulics. A potent tool for modeling and evaluating a broad range of events in numerous domains is COMSOL Multiphysics [22], [23], [24], [25], [26], [27], [28], [29], [30], [31], [32], [33], [34], [35], [36], [37], [38], [39]. Here are a few real-world uses for COMSOL in engineering simulation, [39]:

- **Mechanical Engineering:** COMSOL can simulate stress, strain, and deformation in mechanical components, structural mechanics, geomechanics, and nonlinear material models analyze fluid-structure interaction, and design for optimal performance.
- **Nuclear Engineering:** COMSOL excels at simulating coolant flow, heat transfer, and fuel behavior within the reactor core. This can optimize fuel design, predict core performance, and aid in safety analysis based on thermal hydraulic simulations. Modeling neutron flux, fuel burnup, and control rod behavior is crucial for reactor operation and refueling strategies. COMSOL can be a valuable tool for these simulations. Simulating accident scenarios like loss-of-coolant accidents helps assess safety margins and design emergency cooling systems.
- **Biomedical Engineering:** From designing artificial hearts (left ventricular assist devices) to studying blood flow patterns, COMSOL helps optimize medical devices.
- **Microfluidics:** Design and analyze microfluidic devices used in lab-on-a-chip technologies and medical diagnostics
- **Chemical Engineering:** Model and simulate chemical reactions, mixing processes, and mass transfer in reactors and other chemical equipment
- **Acoustics:** Analyze sound propagation, noise cancellation, and vibration in various applications.

These are just a few examples, and COMSOL's versatility extends to many other fields including aerospace engineering, heat transfer analysis, and material science, [40].

The purpose of this work is to utilize COMSOL Multiphysics tools for the assessment of heat transfer with nanofluids for the passive heat transfer system of the AP1000 reactor.

2 Model

A series of procedures known as the modeling workflow must be followed to set up and operate a finite element model in COMSOL Multiphysics® software. The following steps make up the modeling workflow:

- Constructing the geometry.
- Configuring the environment for the model.
- Describing the characteristics of the materials.
- Assembling the mesh.
- Defining the boundary conditions in physics.
- Putting the simulation into action.
- Modifying the outcomes after they have been obtained.

2.1 Geometry

The geometry option in the Comsol multiphysics software [39] is used to develop a geometry of IRWST of AP1000 under the option model builder. The passive residual heat removing heat exchanging system of the AP1000 reactor design consists of a D-shaped IRWST with a height of 14 m and volume of 2100 m^3 and 689 submerged C-shaped tubes of 5.5 m in length with 19mm in inner radius. To avoid complications in the calculation, a reduced and simplified version of the passive heat-removing system was designed for our study. Figure 1 shows the 3D model of simplified IRWST with a single C-tube. The tank dimensions are reduced to 500 mm in height and 300 mm in radius. The C-tube diameter is given 54 mm to avoid meshing complications. Figure 2 shows the finer mesh of the whole 3D geometry. The flow study and outlet temperature calculation were obtained from the 2D version of the 3D model. After careful examination, every Material property has been chosen in the Settings box for that material.

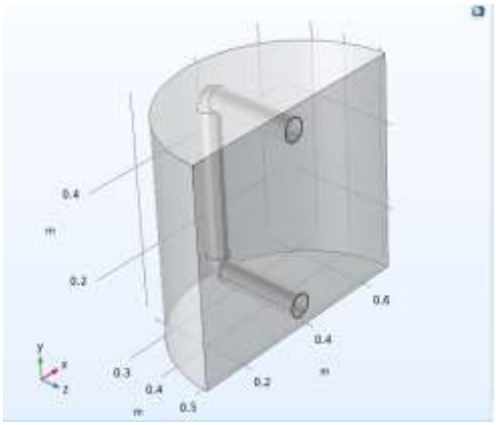

Fig. 1: 3D Model geometry

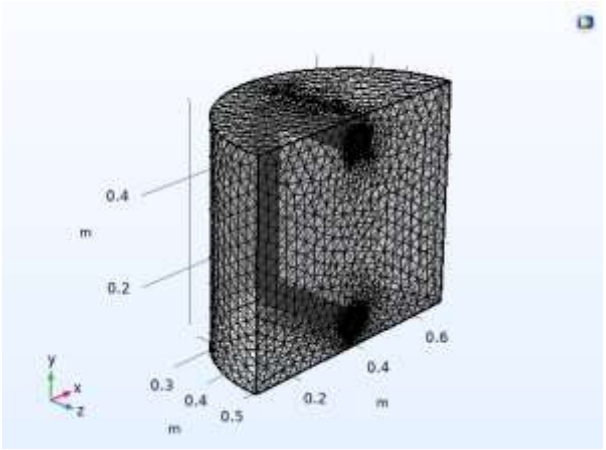

Fig. 2: Mesh of the geometry

2.2 Mesh Quality Analysis

To generate an unstructured tetrahedral mesh, choose User-controlled mesh from the Sequence Type list in the Mesh Settings box. The 3D geometry was studied under 3 different meshing conditions to obtain a comparison between the precision of the results. The physics-controlled mesh conditions were generated automatically by COMSOL. Following are the statistics of each mesh condition over the 3D geometry, [39]. The data on mesh quality and statistics are given in Table 1.

Table 1. Mesh Statistics

Fine mesh	Quality measure	Skewness
	Num. of elements	173071
	Min element quality	0.0782
	Avg element quality	0.6107
	Element volume ratio	6.614e-5
Finer mesh	Quality measure	Skewness
	Num. of elements	836380
	Min element quality	0.1927
	Avg element quality	0.6642
	Element volume ratio	6.128e-5
Extra fine mesh	Quality measure	Skewness
	Num. of elements	1441882
	Min element quality	0.1882
	Avg element quality	0.6717
	Element volume ratio	1.208e-5

Figure 3, Figure 4 and Figure 5 show the 3D geometry under the selected mesh conditions and properties.

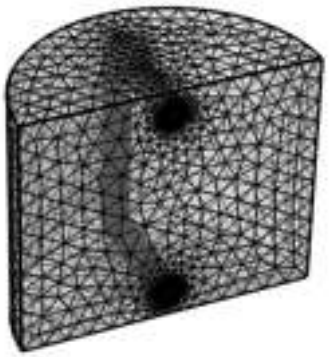

Fig. 3: Fine Mesh

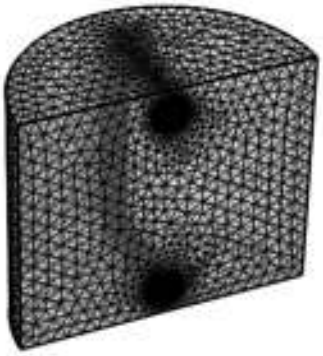

Fig. 4: Finer Mesh

Fig. 5: Extra Fine Mesh

2.3 Boundary Conditions

After that, we check the physics domain settings and establish the heat transfer problem's boundary conditions [39]. The activation temperature for PHRHx of AP1000 design is 297° C and the primary mass flow rate inside the C tubes is 65 kg/s, [23]. The boundary conditions differ from the real scale due to the simplification of the model. Table 2 and Table 3 show the initial and boundary conditions used in both 3D and 2D geometry:

Table 2. Boundary Conditions for Heat Transfer Study (3D)

The initial temperature of IRWST	20°C
The initial temperature of outer temperature at the primary length of the C-tube	20°C
Temperature of primary coolant domain	177°C

Table 3. Boundary Conditions for Flow Study (2D)

The initial temperature of IRWST	20°C
The initial temperature of outer temperature at the primary length of the C-tube	20°C
Temperature of primary coolant inlet	297°C
Inlet velocity	0.001 m/s

3 Methodology

3.1 Simulation

A time-dependent heat transfer study in liquids was performed on the 3D geometry to obtain the selected surface temperature reduction in 100 sec. Figure 6 shows the geometry for the calculation of the heat transfer coefficient. The temperatures were used to calculate the local heat transfer coefficient using theoretical equations. The geometry holds 2 domains- the first one is a primary coolant as the heat source and the other one is the IRWST domain as the heat sink.

Figure 7 shows the selected line for obtaining the heat transfer coefficient. Water and nanofluid properties were added to the material properties of the IRWST domain. To reduce further computational load, a stationary study of heat transfer and laminar flow was done on the 2D geometry to obtain the outlet temperatures. Boundary conditions were adjusted according to the simplifications of the model and studies.

To initiate a simulation, select Compute from the Study option by right-clicking on it in the Model Builder window. A simulation's solution sequence is automatically defined by the Study node based on the chosen study type and physics. In this instance, the simulation can be completed in a matter of seconds. Two convergence graphs are produced during the solution process to display the convergence progress of the various solver algorithms used in the study.

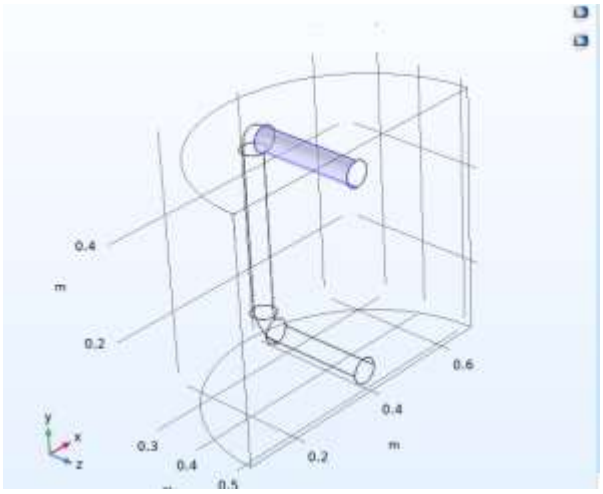

Fig. 6: Selected Surface to Calculate Heat Transfer Coeff

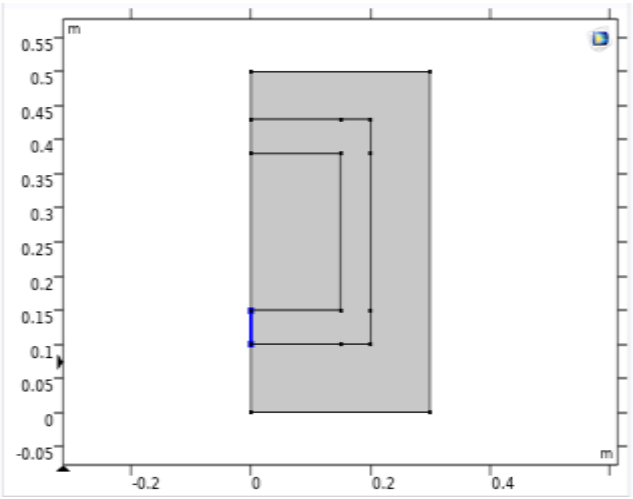

Fig. 7: Selected Line to Obtain Outlet Temperature

Heat Transfer equations used by COMSOL Multiphysics, [39]:

$$\rho C_p \frac{\partial T}{\partial t} + \rho C_p \mathbf{u} \cdot \nabla T + \nabla \cdot \mathbf{q} = Q + Q_{\text{ted}} \quad (1)$$

$$\mathbf{q} = -k \nabla T \quad (2)$$

Where ρ is the fluid density (SI unit: kg/m^3), C_p (SI unit: J/(kg·K)) is the heat capacity at constant pressure, and T (SI unit: K) is the temperature. u is a velocity field, k is the thermal conductivity (SI unit: J/K), and Q (SI unit: W/m) represents a general heat source.

3.2 Calculation of Nanofluid Properties

The thermophysical properties of nanofluid were required to calculate the final heat transfer coefficient. To obtain these properties some experimental and theoretical correlations were implemented. These properties depend on three

main factors- (1) Properties of base fluid (bf) with respect to temperature, (2) Properties of nanoparticles (np) and (3) The volume fraction of nanoparticles mixed in the base fluid. The properties of base fluid water and the Ag, TiO_2, and Al_2O_3 nanoparticles are given in Table 4, [17]. For our study, the different volume fractions of three different nanofluids were considered which are mentioned in Table 5.

Table 4. Properties of Base fluid and Nanoparticles at 300 K

	P (kg/m^3)	**Cp (J/kgK)**	**k (W/mK)**	**β (10^{-5}) (K^{-5})**
Water	997	4179	0.613	21
Ag	10500	235	429	1.89
TiO_2	4250	686.2	8.95	0.9
Al_2O_3	3970	765	40	0.85

Table 5. Percentage of Nanoparticles in Base Fluid

Nanoparticle	**Volume Fraction Considered (Φ)**
Ag	0.25%, 0.5%, 1%
TiO_2	1%, 2%, 3%
Al_2O_3	1%, 3%, 6%

The thermal conductivity (k), viscosity (μ), density (ρ), and specific heat (Cp) for each nanofluid were obtained from the following equations (3), (4), (5), and (6) respectively.

$$k_{nf} = k_{bf}[\frac{k_p+2k_{bf}+2\Phi(k_p-k_{bf})}{k_p+2k_{bf}-\Phi(k_p-k_{bf})}] \quad (3)$$

[Wasp]

$$\mu_{nf} = (1+2.5\Phi)\mu_{bf} \quad (4)$$

$$\rho_{nf} = \Phi\rho_p + (1-\Phi)\rho_{bf} \quad (5)$$

$$C_{p\,nf} = \frac{\Phi\,\rho_p\,C_{p\,p}+(1-\Phi)\rho_{bf}C_{p\,bf}}{\rho_{nf}} \quad (6)$$

3.3 Calculation of Dimensionless Numbers

When the valve of the passive heat removal system opens after 120 sec of reactor shutdown, primary coolant starts to flow in the pipelines connecting to the reactor core and the IRWST. There is a natural circulation of coolant between the core and the submerged heat exchanger pipes due to the temperature and velocity difference. The primary coolant brings residual heat that is still produced in the core to the heat exchanger tubes and the IRWST water absorbs the heat from the outer surface of the pipes. Thus a pool boiling phenomenon occurs in the IRWST which takes about 5 hours to start boiling its water inventory. Another natural circulation of water in the passive heat removing system can be considered in the case of IRWST water boiling.

The calculations of a natural convection heat transfer coefficient calculator usually involve the use of dimensionless number correlations, namely the correlations between the Nusselt number (Nu) and the Rayleigh number (Ra), Grashof number (Gr), and/or Prandtl number (Pr), where Ra = GrPr. The box on the left provides definitions for the Nusselt, Grashof, and Prandtl numbers. The flow regime created by natural convection and the ensuing heat transfer is described by the Rayleigh number (Ra). Considering the natural circulation of the heat sink, the following equations are implemented to calculate Ra, Nu and finally the heat transfer coefficient.

$$Ra = \frac{g\,\beta\,(T_s-T_0)\,L^3}{v^2}\,Pr \quad (7)$$

$$Nu = \{0.6 + \frac{0.387\,Ra^{1/6}}{[\,1+(0.492/Pr)^{9/16}]^{8/27}}\}^2 \quad (8)$$

$$h = \frac{Nu.k}{L} \quad (9)$$

Where:
β- Thermal expansion coefficient of fluid (1/K)
L – characteristic linear dimension (m).
P_r – Prandtl Number of the fluid
v – Kinematic Viscosity (m^2/s)
T_s – Temperature of the solid surface (K)
T_o – Room temperature of the fluid (K)
h- Heat Transfer Coefficient (W/m^2 K)

4 Results and Discussion

The heat transfer coefficient was calculated over the selected surface shown in Figure 6. For each case of nanofluids, a comparison between the heat transfer coefficients depending on the volume concentrations of nanoparticles was plotted in Figure 8, Figure 9 and Figure 10. For all cases, the heat transfer coefficient is found to increase with the increment of the volume fraction of the particles. The heat transfer coefficients in cases of Ag-water nanofluid show comparatively low variance as it is studied in lower mass fraction. On the other hand, for Al_2O_3-water nanofluid, the highest coefficient is found due to the higher thermal conductivity of

Al_2O_3 nanoparticles and its higher mass fraction used in this study which is 6%.

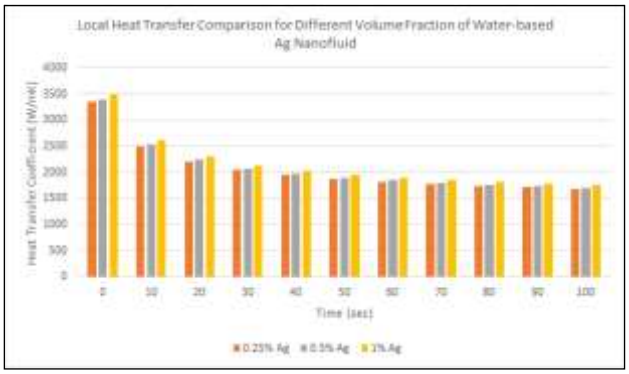

Fig. 8: Local Heat Transfer Comparison for Different Concentrations of Ag-water nf

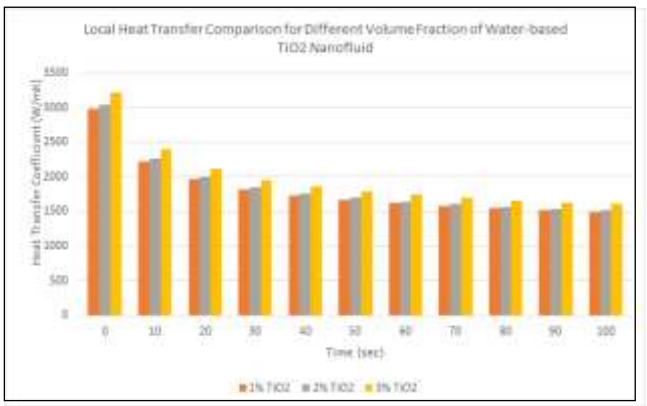

Fig. 9: Local Heat Transfer Comparison for Different Concentrations of TiO_2-water nf

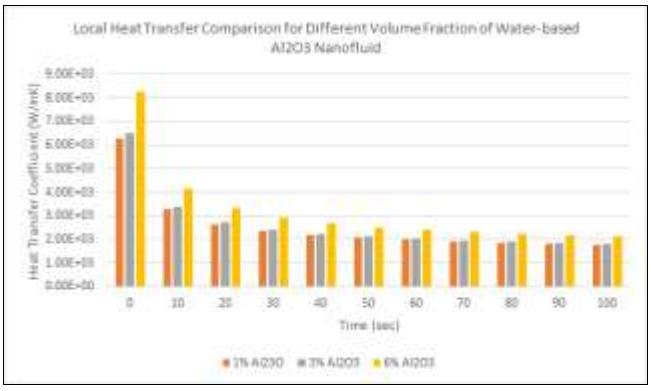

Fig. 10: Local Heat Transfer Comparison for Different Concentrations of Al_2O_3-water nf

The heat transfer performance is enhanced by using nanofluid instead of pure water. The ratio of the heat transfer coefficient of the nanofluids to the base fluid is also studied. Figure 11, Figure 12 and Figure 13 show a comparison of the ratio of heat transfer coefficient of nanofluids in different concentrations. For Ag-water nanofluid the highest ratio is found to be about 1.75 for using the highest concentration considered which only 1% of Ag nanoparticles is. For TiO_2-water nanofluid the highest ratio is 1.6 for the highest concentration 3%. Al_2O_3 showed the best heat transfer coefficient ratio among all the selected nanofluids. For 1% concentration its highest ratio is about 3.2 and for 6% concentration it makes the heat transfer about 6 times higher than pure water.

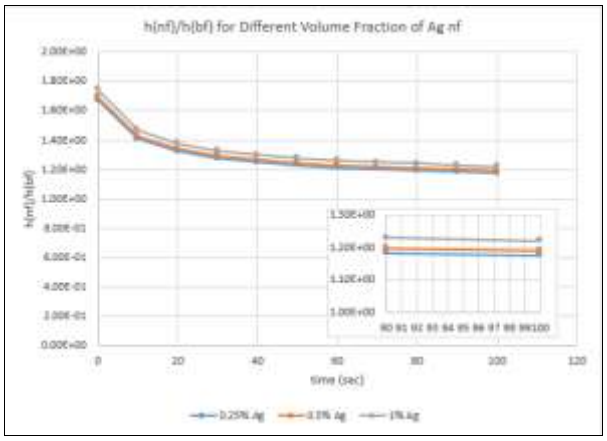

Fig. 11: h(nf)/h(bf) of Ag for Different Volume Fraction

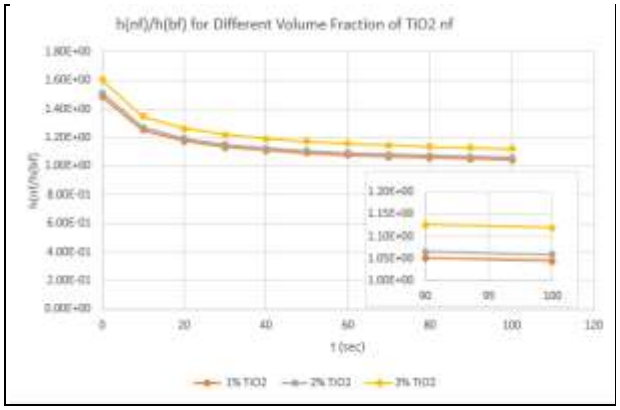

Fig. 12: h(nf)/h(bf) of TiO_2 for Different Volume Fraction

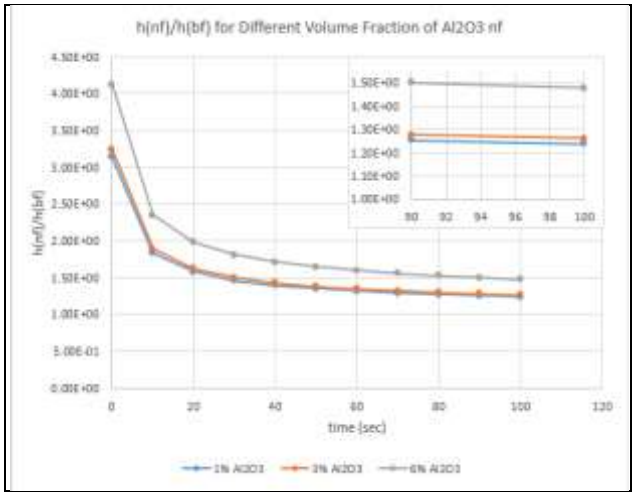

Fig. 13: h(nf)/h(bf) of Al_2O_3 for Different Volume Fraction

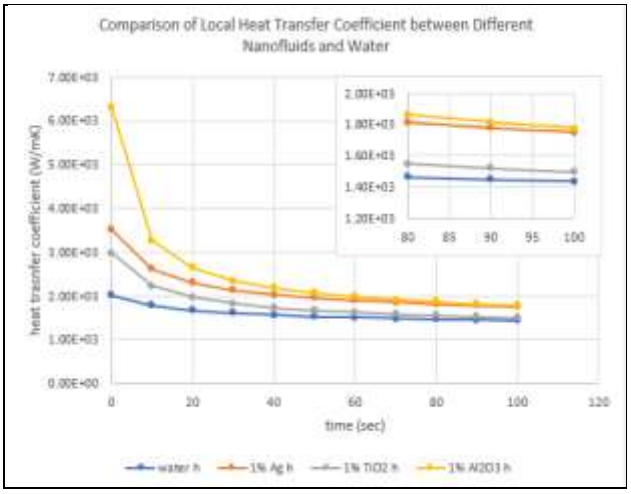

Fig. 14: Comparison Between Heat Transfer Coefficient of Water and Nanofluids

For a better approach to comparing heat transfer performance between water and selected nanofluids, Figure 14 is plotted with the heat transfer coefficient of water and 1% of each nanofluid with respect to time. 1% Al_2O_3 nanofluid shows the highest heat transfer coefficient resulting in a lower outlet temperature of the heat exchanger tube.

From the flow study in 2D geometry, the outlet temperatures were obtained for the cases of water and selected nanofluids as the IRWST inventory. Table 6 gives the simulated outlet temperature when the primary coolant temperature at the inlet is considered to be the activation temperature of the system, i.e., 297°C.

Table 6. Outlet Temperatures

IRWST inventory		**Outlet temperature (°C)**
Water		231.1639
Ag-water	0.25%	231.1028
	0.5%	231.086
	1%	231.0524
TiO2-water	1%	231.064
	2%	231.01
	3%	**230.9489**
Al2O3-water	1%	231.0591
	3%	230.9192
	6%	**230.7028**

The Mesh Independence Test and Convergence Plot are shown in Figure 15 for water. On the other hand, the mesh independence of 6% Ag nanofluid is shown in Figure 16.

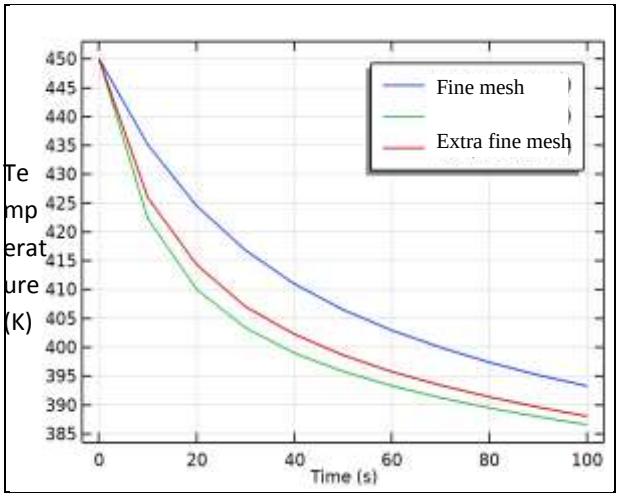

Fig. 15: Mesh Independent Test for Water

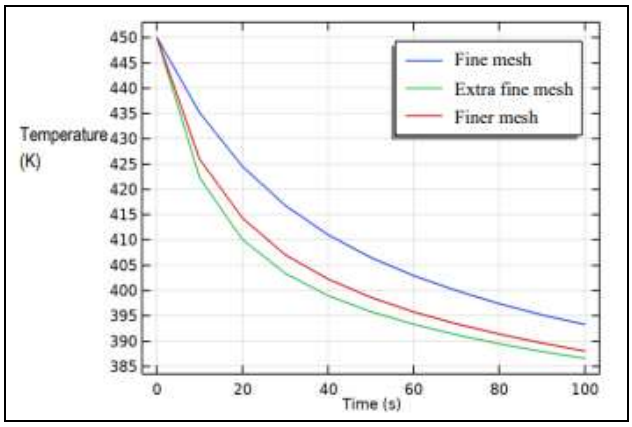

Fig. 16: Mesh-independent Test for 6% Ag Nanofluid

The convergence plot for the stationary study is shown in Figure 17. The convergence plot for the Time Dependent Study is illustrated in Figure 18.

Water as the heatsink study was chosen to demonstrate the convergence as a general representation of the overall computational works.

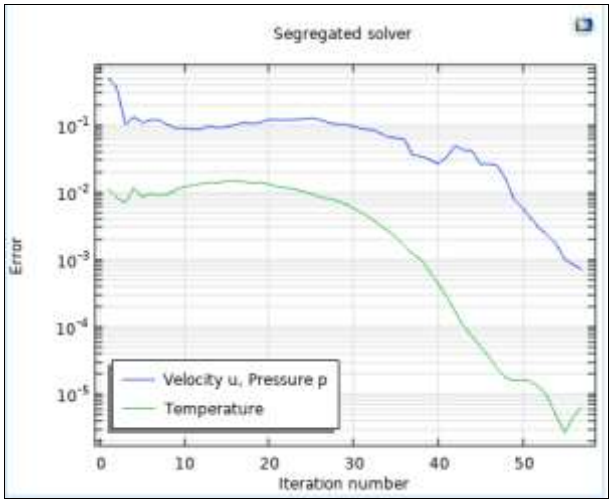

Fig. 17: Convergence Plot for Stationary Study

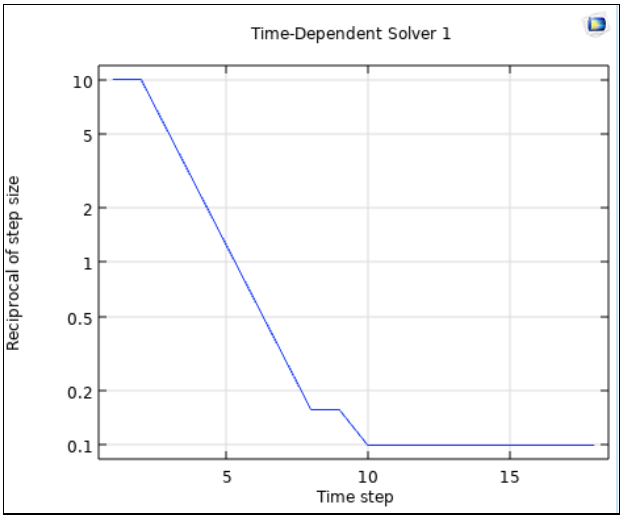

Fig. 18: Convergence Plot for Time Dependent Study

5 Conclusion

This paper deals with a concept of using nanofluid in the IRWST instead of pure water and an investigation on the improved heat transfer coefficient is conducted to illustrate the reduced outlet temperature of the heat exchanger. To avoid computational complications single tube design has been implemented, but the simulation shows an increase in local heat transfer coefficient using the AlO_3 nanofluid. The enhanced thermophysical properties of nanofluid can be a beneficial tool for the passive decay heat removal system for an AP1000 nuclear reactor but the availability and affordability of nanofluid is to be considered. The PRHR HX is an essential part of the PHRS for removing decay heat from the core in case of an emergency and system failure. Using nanofluid to increase the heat transfer efficacy can be a way of enhancing overall safety measurement. Artificial Intelligence (AI) can be integrated with a lot of fascinating studies with nanofluids. Artificial intelligence is outside the scope of this study. This study can be integrated with artificial intelligence (AI) in the future to provide a potent and perceptive research endeavor.

Two VVER-1200 power plants with a combined capacity of 2400 MW will be in operation in Bangladesh by the end of 2024/2025. COMSOL software can be used to simulate the heat transfer of VVER-1200 for safety and licensing purposes but there are challenges to address and future directions to explore.

- COMSOL simulations need validation against actual VVER-1200 data or established reactor physics codes. Access to such data or codes might be limited due to proprietary restrictions.
- Close collaboration with Rosatom (Russia), the VVER-1200 technology provider, would be beneficial. Rosatom might have access to validated simulation data or codes that could be used for COMSOL validation in Bangladesh.
- Developing programs to transfer knowledge and train Bangladeshi researchers and engineers in nuclear simulation techniques and COMSOL software would create a skilled workforce for future nuclear projects.

References:

[1] IAEA Passive Safety Systems and Natural Circulation in Water Cooled Nuclear Power Plants, *IAEA-TECDOC-1624*, IAEA, Vienna 2009, [Online]. https://www-pub.iaea.org/MTCD/publications/PDF/te_1624_web.pdf (Accessed Date: June 15, 2024).

[2] IAEA Passive safety systems in water cooled reactors: an overview and demonstration with basic principle simulators, Training course series no. 69, *International Atomic Energy Agency*, Vienna, 2019, [Online]. https://www-pub.iaea.org/MTCD/Publications/PDF/TCS-69web.pdf (Last Accessed Dates: 15 June 2024).

[3] V.G. Asmolova, I.N. Gusevb, V.R. Kazanskiyb, V.P. Povarovb , D.B. Statsura, New generation first-of-the kind unit – VVER-1200 design features, *Nuclear Energy and Technology*, Vol. 3, Issue 4, 260-269, 2017. https://doi.org/10.1016/j.nucet.2017.10.003.

[4] Yiwa G, Xiongbin L, Ziyi L, Shuliang H, Lanyu Z, Yanfang X, Xiaotian L and Yajun Z (2024), Analysis of transient characteristics and design improvement of the passive residual heat removal system of NHR-200-II. *Front. Energy Res.*, Vol. 12, 1-11, doi: 10.3389/fenrg.2024.1343933.

[5] Status report 81 – Advanced Passive PWR (AP1000), [Online]. https://aris.iaea.org/PDF/AP1000.pdf (Accessed Date: May 22, 2024).

[6] T.L. Schulz, Westinghouse AP1000 advanced passive plant, Nuclear Engineering and Design, Vol. 236 (14-6), 1547-1557, 2006. DOI: 10.1016/j.nucengdes.2006.03.049.

[7] Daogang Lu, Yuhao Z, Zhongyi W, Xiaol Fu, Yanhua Y, and Qiong Cao, Numerical and experimental investigation on the baffle design in secondary side of the PRHR HX in

AP1000, *Annals of Nuclear Energy*, Vol.94, p.359-368, 2016. https://doi.org/10.1016/j.anucene.2016.04.003

[8] Xie X, Nie C, Zhan L, Zheng H, Li P, Tian W, and Pei Yu, Analysis of Heat Transfer and Flow Characteristics of AP1000 Passive Residual Heat Removal Heat Exchanger. *2014 22nd International Conference on Nuclear Engineering*, July 7–11, 2014, Vol. 2B Therm. Hydraul., Prague, Czech Republic. American Society of Mechanical Engineers; 2014, p. V02BT09A061. https://doi.org/10.1115/ICONE22-31230.

[9] Iyahraja S, Rajadurai JS. Study of thermal conductivity enhancement of aqueous suspensions containing silver nanoparticles. *AIP Advances*, Vol. 5, Issue 5, 2015, 5:057103. https://doi.org/10.1063/1.4919808.

[10] Hemmat Esfe M, Saedodin S, Biglari M, Rostamian H. An experimental study on thermophysical properties and heat transfer characteristics of low volume concentrations of Ag-water nanofluid. *Int. Commun. Heat Mass Transf.*, 2016, Vol.74, p.91–7. https://doi.org/10.1016/j.icheatmasstransfer.2016.03.004.

[11] Duangthongsuk W, Wongwises S. Measurement of temperature-dependent thermal conductivity and viscosity of TiO2-water nanofluids. *Exp. Therm. Fluid Sci.*, 2009, Vol.33, p.706–14. https://doi.org/10.1016/j.expthermflusci.2009.01.005.

[12] Eiamsa-ard S, Kiatkittipong K, Jedsadaratanachai W. Heat transfer enhancement of TiO2/water nanofluid in a heat exchanger tube equipped with overlapped dual twisted-tapes. *Eng. Sci. Technol. Int. J.*, 2015, Vol.18, p.336–50. https://doi.org/10.1016/j.jestch.2015.01.008.

[13] Cieśliński JT, Smolen S, Sawicka D. Effect of Temperature and Nanoparticle Concentration on Free Convective Heat Transfer of Nanofluids. *Energies*, 2021, Vol.14, 3566. https://doi.org/10.3390/en14123566.

[14] Akilu S, Sharma KV, Baheta AT, Mamat R. A review of thermophysical properties of water based composite nanofluids. *Renew Sustain. Energy Rev.*, 2016, Vol.66, p.654–78. https://doi.org/10.1016/j.rser.2016.08.036.

[15] S. U. S. Choi and J. A. Eastman, "Enhancing Thermal Conductivity of Fluids with Nanoparticles," In: D. A. Siginer and H. P. Wang, Developments and Applications of Non-Newtonian Flows Eds., *American Society of Mechanical Engineers*, New York, 1995, [Online]. https://ecotert.com/pdf/196525_From_unt-edu.pdf (Accessed Date: July 11, 2024).

[16] Hajatzadeh Pordanjani A, Aghakhani S, Afrand M, Mahmoudi B, Mahian O, Wongwises S. An updated review on application of nanofluids in heat exchangers for saving energy. Energy Convers Manag 2019, Vol.198, 111886. https://doi.org/10.1016/j.enconman.2019.111886.

[17] Tang J. *Numerical investigation of nanofluid flow and heat transfer in flat plate solar collector*, Master of Science Thesis, 2020. The State University of New Jersey, USA, [Online]. https://rucore.libraries.rutgers.edu/rutgers-lib/64915/ (Accessed Date: July 5, 2024).

[18] Park SD, Lee DW, Kang KJ, Park H-S. Numerical study on the thermal-hydraulic behavior in the ultimate heat sink of passive residual heat removal system in the SMART. *Nucl. Eng. Des.*, 2022, Vol.399, 111997. https://doi.org/10.1016/j.nucengdes.2022.111997.

[19] Tao J, Gu H, Xiong Z, Jiang X, Xie Y. Numerical and experimental study on thermal-hydraulic behaviors in the secondary side of passive residual heat removal heat exchanger. *Ann. Nucl. Energy*, 2020, vol.148, 107698. https://doi.org/10.1016/j.anucene.2020.107698.

[20] Liu Y, Mu Z, Wang X, Meng X, Yuan Y, Cao J. Numerical and experimental study of the transient conjugate heat transfer and fluid flow of passive residual heat removal heat exchanger. Int J Therm Sci 2022;181:107726. https://doi.org/10.1016/j.ijthermalsci.2022.107726.

[21] Wu H, Yan L, Yuan L. Pilot numerical study of new design of passive residual heat removal heat exchanger tubes. Prog Nucl Energy 2022, vol.146, 104150. https://doi.org/10.1016/j.pnucene.2022.104150.

[22] Sierchuła J. Analysis of passive residual heat removal system in AP1000 nuclear power plant. *IOP Conf. Ser. Earth. Environ. Sci.*, 2019, vol.214, 012095. https://doi.org/10.1088/1755-1315/214/1/012095.

[23] Lafdaili Z, El-Hamdani S, Bendou A, Limam K, El-Hafad B. Numerical study of the

turbulent natural convection of nanofluids in a partially heated cubic cavity. *Therm. Sci.*, 2021, vol. 25, p.2741–54. https://doi.org/10.2298/TSCI200513057L.

[24] Adnan and W. Ashraf, Heat transfer in tetra-nano-fluid between converging/diverging channel under the influence of thermal radiations by using Galerkin finite element method, *Waves Random Complex Media*, 2023, p.1–16. DOI: 10.1080/17455030.2023.2171154.

[25] Widodo Surip, Nandy Putra, and Anhar Riza Antariksawan, Design of passive residual heat removal systems and application of two-phase thermosyphons: A review, *Progress in Nuclear Energy*, Vol. 154, December 2022, 104473, https://doi.org/10.1016/j.pnucene.2022.104473.

[26] Yanbin Liu, Zhaozhang Mu, Xuesheng Wang, Xiangyu Meng, Yuyang Yuan, and Jiaming Cao, Numerical and experimental study of the transient conjugate heat transfer and fluid flow of passive residual heat removal heat exchanger, *International Journal of Thermal Sciences*, Vol. 181, November 2022, 107726 https://doi.org/10.1016/j.ijthermalsci.2022.107726.

[27] Osman Yücehan Kutlu, *Analysis of VVER-1200 Passive Heat Removal Systems: Steam Generator PHRS and Containment PHRS*, Master's Thesis, May 30, 2019, LUT School of Energy Systems, Lappeenranta University of Technology, Finland, [Online]. https://lutpub.lut.fi/bitstream/handle/10024/163426/Osman_Kutlu_Master_Thesis_final.pdf;jsessionid=80D95ED7B2458866135BFCEB122D9982?sequence=3 (Accessed Date: June 15, 2024).

[28] Lelio Luzzi, Antonio Cammi, Valentino Di Marcello, Carlo Fiorina, An approach for the modelling and the analysis of the MSR thermo-hydrodynamic behavior, *Chemical Engineering Science*, Vol. 65, Issue 16, 2010, p.4873-4883. https://doi.org/10.1016/j.ces.2010.05.040.

[29] Cammi, A., Di Marcello, V., Fiorina, C., Luzzi, L., 2009. Assessment of COMSOL capabilities to analyse the thermo-hydrodynamic behaviour of the MSR core. In: *Proceedings of the COMSOL Conference 2009*, Milan, Italy, CD-ROM, COMSOL, Inc., 2009.

[30] Fiorina, C., 2009. *A generalized approach to assess the COMSOLs capabilities for the analysis of the MSR thermo-fluid dynamics*. M.Sc. Thesis, Politecnico di Milano, Milano, Italy.

[31] M.L.G. Ho, C.S. Oon, L.-L. Tan, Y. Wang, Y.M. Hung, A review on nanofluids coupled with extended surfaces for heat transfer enhancement, *Results in Engineering*, Vol. 17, 2023, 100957. https://doi.org/10.1016/j.rineng.2023.100957.

[32] Ahmed K. Alkaabi and Jeffrey C. King, Benchmarking COMSOL Multiphysics Single-Subchannel Thermal-Hydraulic Analysis of a TRIGA Reactor with RELAP5 Results and Experimental Data, *Science and Technology of Nuclear Installations*, Vol. 2019, Article ID 4375782, 14 pages, https://doi.org/10.1155/2019/4375782.

[33] Trevor K. Howard Prashant K. Jain, *A Verification and Validation Approach for COMSOL Multiphysics to Support the High Flux Isotope Reactor (HFIR)*, July 2021, ORNL/TM-2021/1885, OAK RIDGE NATIONAL LABORATORY, USA.

[34] T. K. Howard, P. Jain, and E. Popov, "Verification and Validation of COMSOL for Heat Transfer in Thin Rectangular Channels Using NACA Test Results," in *18th International Topical Meeting on Nuclear Reactor Thermal Hydraulics, NURETH 2019*, 2019, 8-23 August 2019, Portland, Oregon, USA.

[35] P. K. Jain, J. D. Freels, and D. H. Cook, 3D COMSOL Simulations for Thermal Deflection of HFIR Fuel Plate in the "Cheverton-Kelley" Experiments, ORNL/TM-2012/138, 2012.

[36] Islam, A., R. Nushrat, T.A. Rahim and A.S. Mollah, Modeling and Validation of IAEA 3D PWR Benchmark Problem Using COMSOL Multiphysics Code, *International Journal of Integrated Sciences & Technology*, 4 S (2022) 40-44.

[37] F Ahmed, MA Abir, PK Bhowmik, V Deshpande, A. S. Mollah, D Kumar, Computational assessment of thermo-hydraulic performance of Al_2O_3-water nanofluid in hexagonal rod-bundles subchannel, *Progress in Nuclear Energy*, Vol. 135, 103700, 2021. https://doi.org/10.1016/j.pnucene.2021.103700.

[38] F. Ahmed, Md Minaruzzaman Sumon Muhtasim Fuad, Ravi Gugulothu and A.S. Mollah, Numerical Simulation of Heat exchanger for analyzing the performance of

parallel and counter flow, *WSEAS Transactions on Heat and Mass Transfer*, Vol. 16, 145-152, 2021. https://doi.org/10.37394/232012.2021.16.17.

[39] COMSOL. Introduction to Comsol Multiphysics, [Online]. https://cdn.comsol.com/doc/5.5/IntroductionToCOMSOLMultiphysics.pdf (Accessed Date: July 5, 2024).

[40] COMSOL.The Application Gallery, [Online]. https://www.comsol.com/models (Accessed Date: July 5, 2024).

Contribution of Individual Authors to the Creation of a Scientific Article (Ghostwriting Policy)

- Mantasha Ponkty: Conceptualization, Methodology, Software, Investigation, and Writing - original draft, Review
- Anamika Puja: Modelling, Investigation, Data curation, Writing and Review
- Abdus Sattar Mollah: Conceptualization, Review & Editing, Supervision

Sources of Funding for Research Presented in a Scientific Article or Scientific Article Itself

No funding was received for conducting this study.

Conflict of Interest

The authors have no conflicts of interest to declare.